S-nitrosation of proteins relevant to Alzheimer's disease during early stages of neurodegeneration

Uthpala Seneviratne[a,1], Alexi Nott[b,1], Vadiraja B. Bhat[c], Kodihalli C. Ravindra[a], John S. Wishnok[a], Li-Huei Tsai[b], and Steven R. Tannenbaum[a,d,2]

[a]Department of Biological Engineering, Massachusetts Institute of Technology, Cambridge, MA 02139; [b]The Picower Institute for Learning and Memory, Department of Brain and Cognitive Sciences, Massachusetts Institute of Technology, Cambridge, MA 02139; [c]Agilent Technologies, Inc., Wilmington, DE 19808; and [d]Department of Chemistry, Massachusetts Institute of Technology, Cambridge, MA 02139

Edited by Michael A. Marletta, University of California, Berkeley, CA, and approved February 24, 2016 (received for review October 28, 2015)

Protein *S*-nitrosation (*SNO*-protein), the nitric oxide-mediated posttranslational modification of cysteine thiols, is an important regulatory mechanism of protein function in both physiological and pathological pathways. A key first step toward elucidating the mechanism by which *S*-nitrosation modulates a protein's function is identification of the targeted cysteine residues. Here, we present a strategy for the simultaneous identification of *SNO*-cysteine sites and their cognate proteins to profile the brain of the CK-p25–inducible mouse model of Alzheimer's disease-like neurodegeneration. The approach—*SNO*TRAP (*SNO* trapping by triaryl phosphine)—is a direct tagging strategy that uses phosphine-based chemical probes, allowing enrichment of *SNO*-peptides and their identification by liquid chromatography tandem mass spectrometry. *SNO*TRAP identified 313 endogenous *SNO*-sites in 251 proteins in the mouse brain, of which 135 *SNO*-proteins were detected only during neurodegeneration. *S*-nitrosation in the brain shows regional differences and becomes elevated during early stages of neurodegeneration in the CK-p25 mouse. The *SNO*-proteome during early neurodegeneration identified increased *S*-nitrosation of proteins important for synapse function, metabolism, and Alzheimer's disease pathology. In the latter case, proteins related to amyloid precursor protein processing and secretion are *S*-nitrosated, correlating with increased amyloid formation. Sequence analysis of *SNO*-cysteine sites identified potential linear motifs that are altered under pathological conditions. Collectively, *SNO*TRAP is a direct tagging tool for global elucidation of the *SNO*-proteome, providing functional insights of endogenous *SNO* proteins in the brain and its dysregulation during neurodegeneration.

S-nitrosation | Alzheimer's disease | secretase pathway | presenilin pathway | neurodegeneration

Protein *S*-nitrosation (*SNO*-protein), in which a cysteine (Cys) thiol is converted to a nitrosothiol (RSNO), is an important posttranslational modification (PTM). Cys residues targeted for *S*-nitrosation often impact enzyme activity, protein localization, and protein–protein interactions (1). *SNO* begins with the production of nitric oxide radicals ($NO^{\bullet}$) via conversion of L-arginine to L-citrulline by nitric oxide synthase 1 (NOS1) (neuronal), NOS2 (inducible), and NOS3 (endothelial). NO-mediated *SNO* PTMs are thought to occur in vivo predominantly through radical recombination between $NO^{\bullet}$ and a thiyl radical, transnitrosation by low-molecular weight NO carriers such as *S*-nitrosoglutathione (GSNO), or protein-assisted transnitrosation (2–8). In the healthy brain, low levels of NO and normal *SNO* PTMs play important roles in regulating synaptic plasticity, gene expression, and neuronal survival. In contrast, elevated NO levels associated with aging and environmental stress have been linked to neurological pathologies, including Alzheimer's (AD), Parkinson's, and Huntington's disease (9). AD is the most prevalent form of human dementia, with a frequency that progressively increases in aging societies (10). A pivotal role in development and progression of late-onset AD, and other age-dependent dementias, has been attributed to inflammatory and oxidative stress cascades in the brain (11, 12), which are potentiated by elevated levels of nitrosating and oxidizing species (13, 14).

Despite the biological importance of this PTM, significant gaps exist regarding its in vivo specificity and origin. Characterization of endogenous proteins suggests that not all reduced Cys residues on a given protein and not all Cys-containing proteins are *S*-nitrosated, implying a biased selection. Although *S*-nitrosation has been frequently reported, the specific *SNO* residues for many of the proteins have not been determined and can be critical for determining their function. Currently, the identification of a specific *SNO* residue involves an iterative combination of mutagenic and mass spectrometry (MS)-based approaches. The prototypical method for detecting *SNO*-proteins is the biotin-switch technique (BST), which requires blocking of all free Cys-thiols, followed by selective ascorbate reduction of *SNO*-Cys residues that are biotinylated and isolated for analysis (9, 15–17). One limitation of the BST is that false positives can occur through incomplete blocking of free Cys-thiols, making them difficult to distinguish from true *SNO*-Cys residues. The variability of the BST and similar methods has driven a search for

Significance

Protein *S*-nitrosation (*SNO*-protein) is a posttranslational modification in which a cysteine (Cys) residue is modified by nitric oxide (*SNO*-Cys). *SNO*-proteins impact many biological systems, but their identification has been technically challenging. We developed a chemical proteomic strategy—*SNO*TRAP (*SNO* trapping by triaryl phosphine)—that allows improved identification of *SNO*-proteins by mass spectrometry. We found that S-nitrosation is elevated during early stages of neurodegeneration, preceding cognitive decline. We identified changes in the *SNO*-proteome during early neurodegeneration that are potentially relevant for synapse function, metabolism, and Alzheimer's disease pathology. *SNO*-proteome analysis further reveals a potential linear motif for *SNO*-Cys sites that are altered during neurodegeneration. Our strategy can be applied to multiple cellular and disease contexts and can reveal signaling networks that aid drug development.

Author contributions: U.S., A.N., L.-H.T., and S.R.T. designed research; U.S., A.N., and K.C.R. performed research; U.S., V.B.B., and K.C.R. contributed new reagents/analytic tools; U.S., A.N., K.C.R., J.S.W., L.-H.T., and S.R.T. analyzed data; and U.S., A.N., J.S.W., L.-H.T., and S.R.T. wrote the paper.

The authors declare no conflict of interest.

This article is a PNAS Direct Submission.

Freely available online through the PNAS open access option.

Data deposition: The mass spectrometry proteomics data reported in this paper have been deposited to the ProteomeXchange Consortium, www.ebi.ac.uk/pride/archive via the PRIDE partner repository (accession no. PXD003802).

[1]U.S. and A.N. contributed equally to this work.

[2]To whom correspondence should be addressed. Email: srt@mit.edu.

This article contains supporting information online at www.pnas.org/lookup/suppl/doi:10.1073/pnas.1521318113/-/DCSupplemental.

alternative approaches for accurate *SNO*-Cys detection and mapping.

In this context, we have developed a method that enables global, facile, and high-throughput identification of endogenous *SNO*-Cys residues. *SNO*TRAP (*SNO* trapping by triaryl phosphine) is a direct tagging technique that allows enrichment and identification of *SNO*-proteins and their cognate *SNO*-sites. Hyperactivation of cyclin-dependent kinase-5 (Cdk5) by its activator peptide, p25, leads to AD-like neurodegenerative pathology, and inhibition of p25 activity ameliorates AD phenotypes (18–20). The CK-p25 mouse model of AD-like neurodegeneration allows temporal characterization of neurodegeneration through inducible expression of the p25 activator peptide, leading to elevated amyloid-β levels and DNA damage, followed by synaptic loss, neuronal death, and cognitive impairments (21–24). *SNO*TRAP was used here to profile changes in the *SNO*-proteome of the CK-p25 mouse model of AD-like neurodegeneration and healthy controls (21, 22). Our data provide insights into signaling pathways that may be perturbed by *SNO* in the neurodegenerating brain that could provide novel avenues for AD-related therapies.

Results and Discussion

Site-Specific Identification of *SNO*-Peptides. *SNO*TRAP is a proteomic extension of the method described earlier for detecting low-molecular–weight RSNOs using phosphine ester reagents (25). The *SNO*TRAP probe consists of a triphenylphosphine thioester linked to a biotin molecule through a polyethyleneglycol (PEG) spacer group. The method is based on reaction of the triphenylphosphine thioester with RSNO and subsequent biotin-mediated affinity capture of labeled peptides and/or proteins. The probe reacts with *SNO* groups, first yielding an azaylide intermediate, which through a properly positioned electrophile (thioester), rearranges to form a disulfide–iminophosphorane (Fig. S1*A*) (25, 26). The reaction proceeds through a Staudinger ligation-type mechanism that retains the nitrogen atom and thiol moiety, allowing unequivocal confirmation of specific *SNO*-sites in the peptide. Overall, the workflow consists of three main steps: (*i*) blocking of reduced Cys residues with iodoacetamide (IAM), (*ii*) capture and release of *SNO*-proteins or *SNO*-peptides, and (*iii*) nanoflow liquid chromatography (nLC)–MS/MS analysis (Fig. 1*A*). Blocking with IAM prevents transnitrosation during sample preparation, ensuring that the in vivo location of *SNO*-sites is retained.

To identify *SNO* proteins, and their cognate *SNO*-sites, we used two complementary approaches (Fig. 1*A*). The first was to identify *SNO* proteins, whereby *SNO*TRAP-modified proteins were enriched by streptavidin affinity (Fig. 1*A*, *approach A*). Tryptic peptides were analyzed by LC–MS/MS, and proteins were identified by database searching. Identification of *SNO*-sites using approach A was hindered due to extra features in the mass spectra arising from the *SNO*TRAP tag. These features include (*i*) limited ionization due to the added bulkiness of the triphenylphosphine–PEG–biotin (*SNO*TRAP) tag, (*ii*) added features to the collision-induced dissociation (CID) spectra such as tag-related fragment ions and corresponding neutral losses, and (*iii*) ion suppression by the dominant ions created by the *SNO*TRAP tag.

Consequently, a second approach (B) was developed that substitutes *N*-ethyl maleimide (NEM) for the bulky *SNO*TRAP tag, which allows direct detection of *SNO*-sites by MS. Briefly, proteolytic digestion is performed before streptavidin capture to isolate modified peptide fragments that contain the *SNO*TRAP tag rather than intact *SNO*-proteins. (Fig. 1*A*, *approach B*). The *SNO*TRAP tag is subsequently cleaved, the peptides eluted with triscarboxyethylphosphine (TCEP), and the liberated Cys labeled with NEM before nLC–MS/MS. This strategy selectively enriches only *SNO*-containing peptides, which reduces the complexity of the nLC separation and improves the detection of *SNO*-sites. The diagnostic fragment ions (DFIs) at *m/z* 126.0550, 125.0477, and 158.0276 verify that this was a *SNO*-peptide

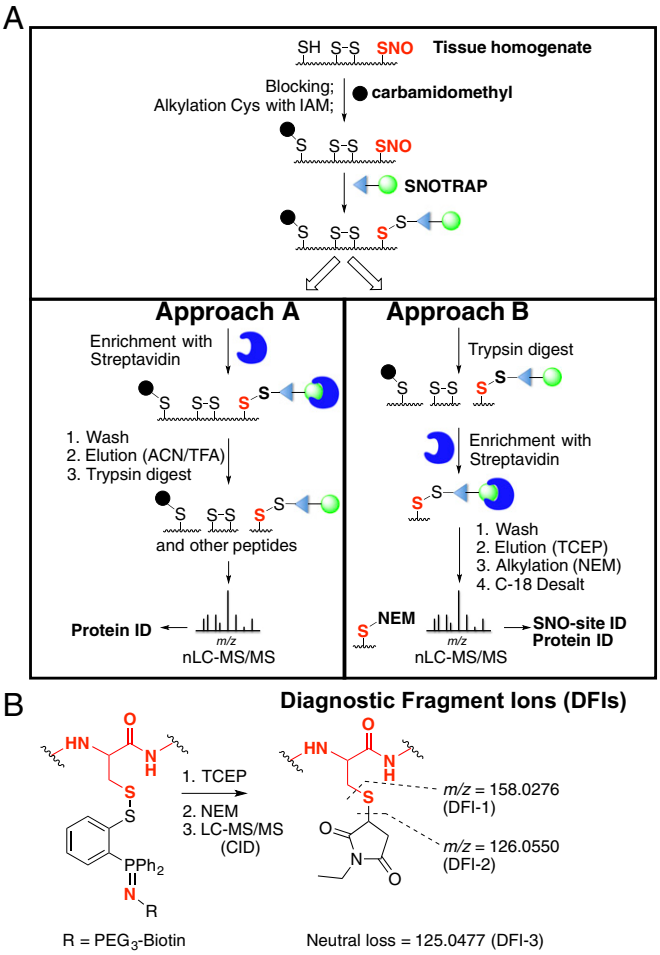

Fig. 1. Site-specific identification of *SNO*-protein. (*A*) Schematic for selective labeling and analysis of *SNO*-proteins. Unmodified Cys-thiols were blocked, and *SNO*-Cys sites were labeled with the *b-SNO*TRAP probe. For approach A, *b-SNO*TRAP–tagged proteins were enriched using streptavidin beads, washed, eluted with denaturing conditions, trypsin-digested, and analyzed by LC–MS/MS. For approach B, the proteome was trypsin-digested, and *b-SNO*TRAP–tagged peptides were enriched using streptavidin beads, followed by release of the biotin linker by TCEP; alkylated with NEM; and analyzed by LC–MS/MS. (*B*) Generation of DFIs from NEM-modified peptides.

(Fig. 1*B* and Fig. S1*B*) (27, 28). Our criteria for identification of *SNO*-proteins required detection of two or more tryptic peptides per *SNO*-protein using approach A and the *SNO*-Cys site-specific peptide identification using approach B.

Cortical tissues from CK-p25 mice were analyzed independently by capture of *SNO*-proteins (approach A) and *SNO*-peptides (approach B), using multiple biological replicates. Proteins were identified by Spectrum Mill (Agilent) for both approaches and pooled for analysis. By matching peptides for a given protein using a combination of both approaches, we identified 251 proteins (Dataset S1). DFIs in MS/MS spectra using approach B pinpointed 313 *SNO*-sites within these proteins (Dataset S1; MS/MS spectra can be viewed at web.mit.edu/toxms/www/SNOTRAP/). Detection of *SNO*-glyceraldehyde-3-phosphate dehydrogenase (GAPDH) on Cys-150, as previously reported by others using independent approaches, validated the robustness of the protocol (Fig. S1 *B* and *C*) (16, 29). *SNO*TRAP also detected previously unidentified *SNO*-sites, such as *SNO*-Cys284 of gephyrin (GPHN1), indicating the sensitivity of the method (Fig. S1 *B* and *C*). The *SNO*TRAP approach was able to detect and identify a large number of endogenous *SNO*-proteins and *SNO*-sites in the brain and is

complementary to previous reports for mouse, rat, and human (Fig. S1*F*) (16, 30–32).

To control for false positives that may result from nonspecific interactions with the streptavidin beads, pretreatment with TCEP, UV, and ascorbate-Cu were used to displace *SNO* PTMs before reaction with the *SNO*TRAP probe and analyzed by MS (Fig. S1*D*). Samples pretreated with TCEP were also analyzed by Western blot (Fig. S1*E*). Approximately 3% of peptides and 5% of proteins (*Materials and Methods*) were identified as false positives (present in both the test samples and negative controls) and were removed from further analysis.

***SNO*-Proteins Identified During Early Neurodegeneration.** To determine temporal changes during neurodegeneration of *SNO*-proteins and their cognate *SNO*-Cys sites, we used the CK-p25 mouse model of AD-like neurodegeneration. CK-p25 mice show early signs of neurodegeneration, including DNA damage, increased amyloid-β, and the onset of neuroinflammation, before behavior abnormalities (Fig. 2*A*) (21, 22, 33). After 6 wk of p25 induction, mice exhibit learning and memory impairments and signs of advanced neurodegeneration, such as neuronal death and reduced synapse number (23, 24). To assess changes in *SNO* in the brain during the progression of neurodegeneration, we first measured GSNO levels in the hippocampus, cortex, and cerebellum of CK-p25 mice and p25 control littermates during early (2 wk) and later (6 wk) stages of neurodegeneration. In control mice, the levels of GSNO were highest in the cerebellum, reflecting previous observations that NOS1 expression is high in the cerebellum of adult mice (13). During early stages of neurodegeneration, GSNO increased in the cortex and the hippocampus to levels (twofold and threefold, respectively) that either resembled or surpassed that of the cerebellum (Fig. 2*B*). Increased *SNO* levels in 2-wk–induced CK-p25 mice correlate with elevated DNA damage previously observed in these regions (24). In the cerebellum, no increase in GSNO was observed at 2 wk, which likely reflects the low level of p25 induction in this brain region (21). GSNO levels in the hippocampus and cortex during a later stage of neurodegeneration return to levels similar to controls. Low levels of NO lead to *S*-nitrosation, whereas high levels cause cell death (14). The reduction of GSNO levels at a later stage of neurodegeneration could reflect a change in the proportion of cell types in these regions, including a loss of neurons and gliosis (21), although the possibility of lowered *SNO* production cannot be excluded. Collectively, our results suggest that elevated GSNO in the hippocampus and cortex is an early indicator of neurodegeneration and that elevated *SNO* may be a driving mechanism for disease progression.

To assess the endogenous *SNO*-proteome profile in the brains of CK-p25 and control mice during early stages of neurodegeneration (2 wk), *SNO*-proteins were isolated and identified in the cortex, hippocampus, and cerebellum. We detected a larger number of *SNO*-proteins and *SNO*-sites in CK-p25 mice compared with controls. In control mice, 152 *SNO*-sites and 116 *SNO*-proteins were identified, compared with 292 *SNO*-sites and 237 *SNO*-proteins in the CK-p25 mice (Dataset S1). The largest increase in CK-p25–specific *SNO*-proteins was detected in the cortex (Fig. 2*C*), which is consistent with elevated levels of GSNO during early neurodegeneration (Fig. 2*B*). Of the 212 *SNO*-proteins identified in the cortex, almost two-thirds (64%) were detected only in the CK-p25 mice (Fig. 2*C* and Dataset S1). A total of 264 *SNO*-Cys sites were identified in the cortex, of which 160 (61%) were found exclusively in CK-p25 mice (Dataset S1).

We detected 89 *SNO*-proteins in the hippocampus. Although AD pathology is readily observed in the hippocampus and our data show elevated GSNO, the majority of detected *SNO*-proteins (70%) were common between CK-p25 and controls (Fig. 2*C*). The reduced number of proteins may reflect a limitation in the total protein we obtained from the hippocampus (Fig. 2*C* and Dataset

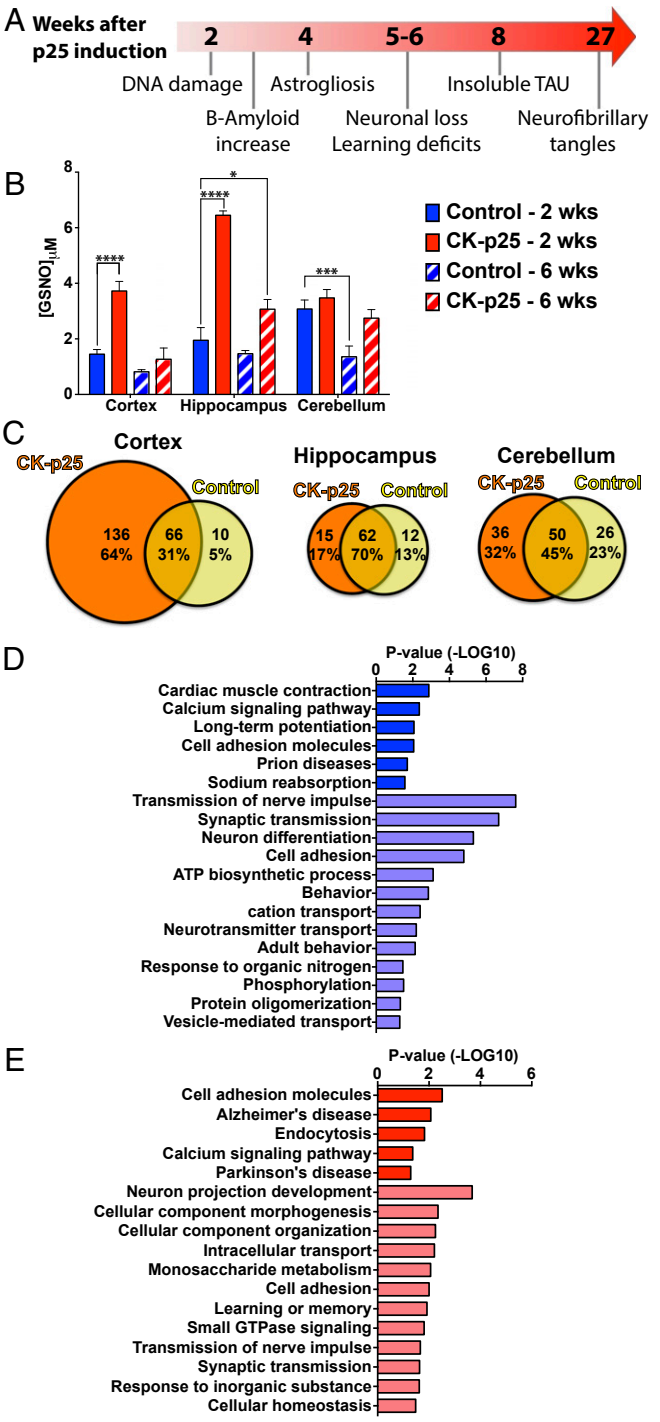

Fig. 2. Altered levels of *SNO* are detected in CK-p25 mice during early stages of neurodegeneration. (*A*) Timeline of the pathological progression of the CK-p25 mouse model of neurodegeneration. (*B*) GSNO concentration (μM) in the cortex, hippocampus, and cerebellum of control or CK-p25 mice following induction of p25 expression for 2 wk or 6 wk. Two-way ANOVA; Dunnett's multiple comparisons; $^{****}P < 0.0001$, $^{***}P < 0.001$, $^{*}P < 0.05$; $n = 4$ for 2-wk samples and $n = 3$ for 6-wk samples; mean ± SEM. (*C*) Number of *SNO*-proteins identified in the cortex, hippocampus, and cerebellum of control and CK-p25 mice following 2-wk induction. (*D*) Gene ontology analysis of total *SNO*-proteins identified in the cortex of control mice (dark blue, KEGG pathways; light blue, BPs). (*E*) Gene ontology analysis of *SNO*-proteins exclusively identified in the cortex of CK-p25 mice following 2-wk induction (dark red, KEGG pathways; light red, BPs).

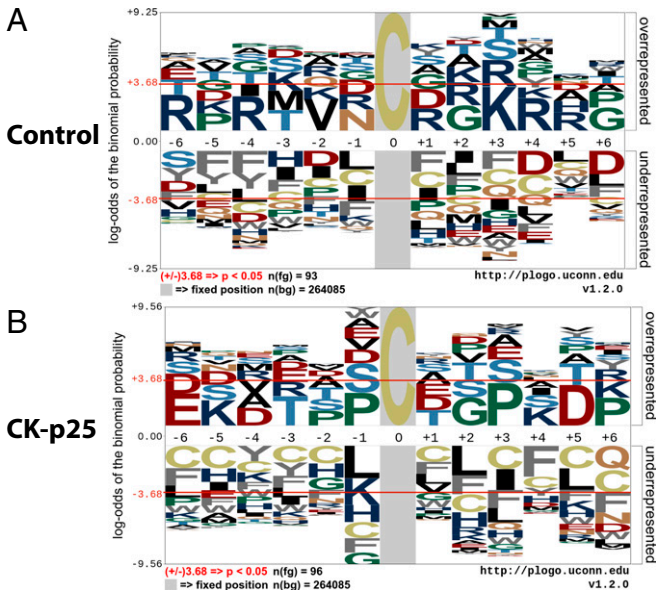

Fig. 3. *SNO*-site linear motif analysis indicates differential preference for *SNO*-Cys sites during early neurodegeneration. (*A*) Linear motif generated by pLOGO using sequences flanking *SNO*-Cys sites detected in control mice. (*B*) Linear motif generated by pLOGO using sequences flanking *SNO*-Cys sites exclusively detected in 2-wk–induced CK-p25 mice.

S1). The cerebellum has an approximately equal distribution of *SNO*-proteins (32%, 45%, and 23%) between control and CK-p25 mice (Fig. 2*C* and Dataset S1) and mirrors observations of little change in GSNO for this brain region (Fig. 2*B*).

Bioinformatic Analysis of the *S*-Nitrosoproteome. To decipher the possible impact of *SNO*-proteins on molecular and cellular systems during early neurodegeneration, we performed gene ontology analysis of biological processes (BPs) and KEGG pathways using the total control *SNO*-proteome (Fig. 2*D*) and the CK-p25–specific *SNO*-proteome (Fig. 2*E*) of the cortex (34, 35). Gene ontology clusters associated with synaptic functions were observed for *SNO*-proteins in control and CK-p25 mice (BP_Synaptic transmission and BP_Transmission of nerves impulse). The synaptic protein synaptophysin was validated by *SNO*TRAP-Western blot (Fig. S2*A*). Pathways associated with cognition were identified in both control (KEGG_Long-term potentiation and BP_Behavior) and CK-p25 mice (BP_Learning or memory). Collectively, these data suggest that regulation of synaptic *SNO*-proteins is important for normal neuronal functions associated with learning and memory and also that the synapse is vulnerable to aberrant *SNO*-signaling. NOS1, the major source of neuronal NO, is tethered to the synapse by postsynaptic density protein 95 (PSD95; also known as DLG4) (36). Although we did not detect *SNO*-PSD95 by MS, *SNO*TRAP-Western blot analysis shows a strong elevation of *SNO*-PSD95 in CK-p25 mice (Fig. S2*B*), indicating a susceptibility of the synapse to increased *SNO* during early neurodegeneration.

SNO-proteins linked to AD were detected in the CK-p25 cortex and not in controls, as identified by the AD KEGG pathway (Fig. 2*E*; GRIN2B, TAU, GSK3β, LRP1, NDUFS1, COX6B1, and GAPDH). NOS1 is activated by *N*-methyl-D-aspartate receptor (NMDAR)-mediated influx of Ca^{2+}; subsequent *S*-nitrosation of NMDAR is thought to modulate its activity. However, hyperexcitation of NMDAR leads to excessive Ca^{2+} signaling and elevated NO production, conditions thought to occur during neurodegeneration. This could explain detection of *SNO*-GRIN2B, a subunit of the NMDAR, in the CK-p25 mice. Amyloid activation of the NMDAR can increase p25 production, possibly providing a feed-forward mechanism for *SNO* production (18). NMDAR-mediated p25 production and Cdk5 activation is thought to increase glycogen synthase kinase-3β (GSK3β) and TAU (Mapt) phosphorylation, two key mediators of neuronal death in AD, both of which we identified in the CK-p25 mice. Elevated *SNO*-GSK3β was validated by *SNO*TRAP-Western blot analysis (Fig. S2*A*). Cdk5 itself has been reported to be *S*-nitrosated, which enhances its serine/threonine kinase activity (37). Although *SNO*-Cdk5 was not detected by MS, it was elevated in CK-p25 mice (shown by *SNO*TRAP-Western blot; Fig. S2*B*), possibly contributing to elevated Cdk5 activity and acting as a feed-forward mechanism during neurodegeneration. In addition, protein kinase C (PKC) epsilon and gamma isoforms (Prkce and Prkcg) were *S*-nitrosated in CK-p25 mice. PKC inhibits GSK3β and promotes nonamyloidogenic processing of amyloid precursor protein (APP) through activation of α-secretase (38). *S*-nitrosation inhibits PKC activity (39, 40) and therefore may reduce APP processing through the nonamyloidogenic α-secretase pathway.

Additional AD-related pathways impacted by *SNO* during neurodegeneration included apolipoprotein E (ApoE)-mediated amyloid clearance (*SNO*-LRP1) and mitochondrial dysfunction (*SNO*-NDUFS1 and *SNO*-COX6B1, which are components of CxI and CxIV of the respiratory chain). Furthermore, Gene Ontology (GO) analysis indicated that proteins regulating glycolysis were enriched in the CK-p25–specific *SNO*-proteome (BP_Monosaccharide metabolism), suggesting that elevated *SNO* may affect metabolic processes during early neurodegeneration. In particular, GAPDH was *S*-nitrosated in CK-p25 mice but not in control mice and was validated by *SNO*TRAP-Western blot (Fig. S2*A*). Nuclear *SNO*-GAPDH transnitrosates SIRT1, HDAC2, and DNA-PK (DNA-dependent protein kinase, catalytic subunit), impacting metabolic pathways, aging, and chromatin remodeling (41–43). HDAC2 was not detected in our *SNO*-proteome, although we observed elevated *SNO*-HDAC2 in CK-p25 mice by *SNO*TRAP-Western blot (Fig. S2*B*).

Linear Motifs for *S*-Nitrosation. Recent studies indicate that the specificity of *SNO*-Cys sites may be dependent on the spatial proximity of charged amino acids, which are hypothesized to

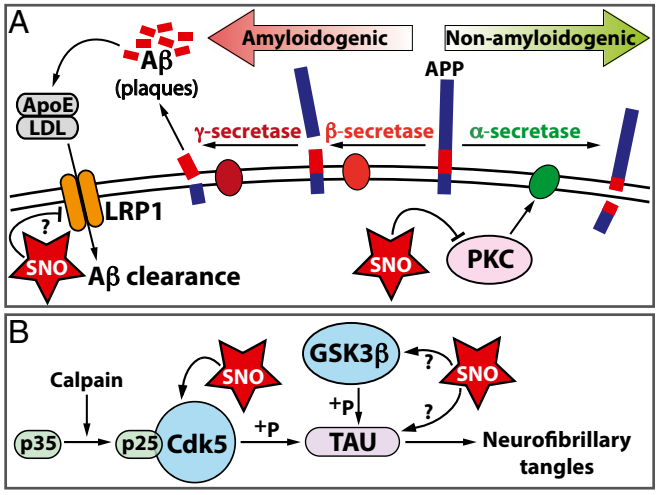

Fig. 4. Pathways affected by *S*-nitrosation during neurodegeneration. (*A*) *SNO*-LRP1 and *SNO*-PKC isoforms were identified in CK-p25 mice after 2-wk induction and have been implicated in secretase processing of APP and amyloid clearance. (*B*) *SNO*-GSK3β and *SNO*-TAU were identified in CK-p25 mice after 2-wk induction and have been implicated in neurofibrillary tangle formation and AD pathology. The functional implications of previously unidentified SNO-proteins are represented with a question mark.

allow protein–protein interactions that facilitate transnitrsation (29, 44). To elucidate common features of *SNO*-Cys sites, we used the probability LOGO (pLOGO) tool to analyze flanking sequences of *SNO*-Cys residues for linear motifs (45). Motif analysis of SNO-Cys sites in control and CK-p25 mice revealed an overrepresentation of charged flanking amino acids; however, this was not consistent for all SNO-Cys sites (Fig. 3 *A* and *B*). Specifically, in control mice, basic residues Arg (R) and Lys (K) were overrepresented at the –6, –4, +1, +3, +4, and +5 positions (Fig. 3*A*); these residues may be required for base-catalyzed transnitrosation (1, 46). To test the robustness of the motif, we performed pLOGO analysis using an independently published *SNO*-proteome from brains of wild-type (C57BL/6J) mice (47) and found an enrichment of the basic residues—Lys (K), Arg (R), and His (H)—surrounding the *SNO*-Cys position (Fig. S2*C*, –6, –5, –1, +3, and +4). In the CK-p25 mice, we observed Lys (K) basic residues at the –5 and +4 positions and Glu (E) and Asp (D) acidic residues at the –6, –4, and +5 positions (Fig. 3*B*). This motif may represent charge clustering and has been previously proposed to allow acid–base catalysis for nitrosation (base) and denitrosation (acid) of Cys residues. Despite these observations, many *SNO*-Cys sites identified in both control and CK-p25 mice did not have charged amino acids within a proximal location of the primary sequence. Previous studies indicate that tertiary structural elements may be required for localizing charged residues to SNO-Cys sites for many proteins (29, 44). Collectively, these data suggest that the specificity for *S*-nitrosation of a subset of Cys may be dependent on proximal charged amino acids, which possibly provide docking sites for nitrosating and denitrosating agents (29).

Conclusion

Through development of *SNO*TRAP, a direct *SNO*-tagging MS method for detecting both small and large molecular RSNOs, we identified an expanded endogenous *SNO*-proteome in the mouse brain. We identified the hippocampus and cortex as regions subjected to elevated levels of *SNO* during early stages of neurodegeneration that precede the onset of detrimental behavioral changes. The identification of *SNO*-PKC and *SNO*-LRP1 during neurodegeneration suggests that elevated *SNO* may impact amyloid processing and clearance, thus contributing to amyloid plaque deposition (Fig. 4*A*). Furthermore, detection of *SNO*-GSK3β and *SNO*-TAU in the CK-p25 mice indicates that aberrant *SNO* signaling may affect neurofibrillary tangle formation, another hallmark of AD pathology (Fig. 4*B*). The susceptibility of multiple proteins to *S*-nitrosation during early neurodegeneration relevant to synaptic function, metabolism, and AD pathology may drive cellular pathologies observed at later stages, such as neuronal loss, reduced synapse integrity, and ultimately memory impairment (Fig. 4 *A* and *B*). Increased protein aggregation and cell death linked to *SNO*-proteins in CK-p25 mice likely lead to activation of inflammatory responses, an important component of AD pathology and progression (33). The *SNO*TRAP strategy provided a comprehensive assessment of *S*-nitrosation in the neurodegenerating brain that can be applied to multiple cellular and disease contexts and has therapeutic potential for biomarker discovery and drug development.

Animals. All mouse experiments were approved by the Committee on Animal Care of the Division of Comparative Medicine at Massachusetts Institute of Technology.

ACKNOWLEDGMENTS. This work was supported by National Institutes of Health Grant CA26731, MIT Center for Environmental Health Sciences Grant ES002109, a grant from the Simons Foundation to the Simons Center for the Social Brain at MIT (S.R.T.), and National Institutes of Health Grant R01 NS051874 (to L.-H.T.).

1. Hess DT, Matsumoto A, Kim SO, Marshall HE, Stamler JS (2005) Protein S-nitrosylation: Purview and parameters. *Nat Rev Mol Cell Biol* 6(2):150–166.
2. Smith BC, Marletta MA (2012) Mechanisms of S-nitrosothiol formation and selectivity in nitric oxide signaling. *Curr Opin Chem Biol* 16(5-6):498–506.
3. Martínez-Ruiz A, Cadenas S, Lamas S (2011) Nitric oxide signaling: Classical, less classical, and nonclassical mechanisms. *Free Radic Biol Med* 51(1):17–29.
4. Keshive M, Singh S, Wishnok JS, Tannenbaum SR, Deen WM (1996) Kinetics of S-nitrosation of thiols in nitric oxide solutions. *Chem Res Toxicol* 9(6):988–993.
5. Keszler A, Zhang Y, Hogg N (2010) Reaction between nitric oxide, glutathione, and oxygen in the presence and absence of protein: How are S-nitrosothiols formed? *Free Radic Biol Med* 48(1):55–64.
6. Madej E, Folkes LK, Wardman P, Czapski G, Goldstein S (2008) Thiyl radicals react with nitric oxide to form S-nitrosothiols with rate constants near the diffusion-controlled limit. *Free Radic Biol Med* 44(12):2013–2018.
7. Mitchell DA, Marletta MA (2005) Thioredoxin catalyzes the S-nitrosation of the caspase-3 active site cysteine. *Nat Chem Biol* 1(3):154–158.
8. Seth D, Stamler JS (2011) The SNO-proteome: Causation and classifications. *Curr Opin Chem Biol* 15(1):129–136.
9. Nakamura T, et al. (2015) Aberrant protein S-nitrosylation contributes to the pathophysiology of neurodegenerative diseases. *Neurobiol Dis* 84:99–108.
10. Abbott A (2012) Cognition: The brain's decline. *Nature* 492(7427):S4–S5.
11. Agostinho P, Cunha RA, Oliveira C (2010) Neuroinflammation, oxidative stress and the pathogenesis of Alzheimer's disease. *Curr Pharm Des* 16(25):2766–2778.
12. Sultana R, Butterfield DA (2010) Role of oxidative stress in the progression of Alzheimer's disease. *J Alzheimers Dis* 19(1):341–353.
13. Bredt DS, Snyder SH (1994) Transient nitric oxide synthase neurons in embryonic cerebral cortical plate, sensory ganglia, and olfactory epithelium. *Neuron* 13(2): 301–313.
14. Dedon PC, Tannenbaum SR (2004) Reactive nitrogen species in the chemical biology of inflammation. *Arch Biochem Biophys* 423(1):12–22.
15. Forrester MT, et al. (2009) Proteomic analysis of S-nitrosylation and denitrosylation by resin-assisted capture. *Nat Biotechnol* 27(6):557–559.
16. Hao G, Derakhshan B, Shi L, Campagne F, Gross SS (2006) SNOSID, a proteomic method for identification of cysteine S-nitrosylation sites in complex protein mixtures. *Proc Natl Acad Sci USA* 103(4):1012–1017.
17. Jaffrey SR, Erdjument-Bromage H, Ferris CD, Tempst P, Snyder SH (2001) Protein S-nitrosylation: A physiological signal for neuronal nitric oxide. *Nat Cell Biol* 3(2): 193–197.
18. Seo J, et al. (2014) Activity-dependent p25 generation regulates synaptic plasticity and Aβ-induced cognitive impairment. *Cell* 157(2):486–498.
19. Shukla V, et al. (2013) A truncated peptide from p35, a Cdk5 activator, prevents Alzheimer's disease phenotypes in model mice. *FASEB J* 27(1):174–186.
20. Shukla V, Skuntz S, Pant HC (2012) Deregulated Cdk5 activity is involved in inducing Alzheimer's disease. *Arch Med Res* 43(8):655–662.
21. Cruz JC, Tseng H-C, Goldman JA, Shih H, Tsai L-H (2003) Aberrant Cdk5 activation by p25 triggers pathological events leading to neurodegeneration and neurofibrillary tangles. *Neuron* 40(3):471–483.
22. Cruz JC, et al. (2006) p25/cyclin-dependent kinase 5 induces production and intraneuronal accumulation of amyloid beta in vivo. *J Neurosci* 26(41):10536–10541.
23. Fischer A, Sananbenesi F, Pang PT, Lu B, Tsai L-H (2005) Opposing roles of transient and prolonged expression of p25 in synaptic plasticity and hippocampus-dependent memory. *Neuron* 48(5):825–838.
24. Kim D, et al. (2008) Deregulation of HDAC1 by p25/Cdk5 in neurotoxicity. *Neuron* 60(5):803–817.
25. Seneviratne U, Godoy LC, Wishnok JS, Wogan GN, Tannenbaum SR (2013) Mechanism-based triarylphosphine-ester probes for capture of endogenous RSNOs. *J Am Chem Soc* 135(20):7693–7704.
26. Zhang J, Wang H, Xian M (2009) An unexpected Bis-ligation of S-nitrosothiols. *J Am Chem Soc* 131(11):3854–3855.
27. Levsen K, et al. (2005) Structure elucidation of phase II metabolites by tandem mass spectrometry: An overview. *J Chromatogr A* 1067(1-2):55–72.
28. Yang J, Gupta V, Carroll KS, Liebler DC (2014) Site-specific mapping and quantification of protein S-sulphenylation in cells. *Nat Commun* 5:4776.
29. Doulias P-T, et al. (2010) Structural profiling of endogenous S-nitrosocysteine residues reveals unique features that accommodate diverse mechanisms for protein S-nitrosylation. *Proc Natl Acad Sci USA* 107(39):16958–16963.
30. Doulias P-T, Tenopoulou M, Greene JL, Raju K, Ischiropoulos H (2013) Nitric oxide regulates mitochondrial fatty acid metabolism through reversible protein S-nitrosylation. *Sci Signal* 6(256):rs1.
31. Zahid S, Khan R, Oellerich M, Ahmed N, Asif AR (2014) Differential S-nitrosylation of proteins in Alzheimer's disease. *Neuroscience* 256:126–136.
32. Zaręba-Kozioł M, Szwajda A, Dadlez M, Wysłouch-Cieszyńska A, Lalowski M (2014) Global analysis of S-nitrosylation sites in the wild type (APP) transgenic mouse brain-clues for synaptic pathology. *Mol Cell Proteomics* 13(9):2288–2305.
33. Gjoneska E, et al. (2015) Conserved epigenomic signals in mice and humans reveal immune basis of Alzheimer's disease. *Nature* 518(7539):365–369.
34. Huang W, Sherman BT, Lempicki RA (2009) Systematic and integrative analysis of large gene lists using DAVID bioinformatics resources. *Nat Protoc* 4(1):44–57.
35. Mi H, Muruganujan A, Casagrande JT, Thomas PD (2013) Large-scale gene function analysis with the PANTHER classification system. *Nat Protoc* 8(8):1551–1566.

36. Christopherson KS, Hillier BJ, Lim WA, Bredt DS (1999) PSD-95 assembles a ternary complex with the N-methyl-D-aspartic acid receptor and a bivalent neuronal NO synthase PDZ domain. *J Biol Chem* 274(39):27467–27473.
37. Qu J, et al. (2011) S-Nitrosylation activates Cdk5 and contributes to synaptic spine loss induced by beta-amyloid peptide. *Proc Natl Acad Sci USA* 108(34):14330–14335.
38. de Barry J, Liégeois CM, Janoshazi A (2010) Protein kinase C as a peripheral biomarker for Alzheimer's disease. *Exp Gerontol* 45(1):64–69.
39. Choi H, Tostes RC, Webb RC (2011) Thioredoxin reductase inhibition reduces relaxation by increasing oxidative stress and s-nitrosylation in mouse aorta. *J Cardiovasc Pharmacol* 58(5):522–527.
40. Gopalakrishna R, Chen ZH, Gundimeda U (1993) Nitric oxide and nitric oxide-generating agents induce a reversible inactivation of protein kinase C activity and phorbol ester binding. *J Biol Chem* 268(36):27180–27185.
41. Hara MR, et al. (2005) S-nitrosylated GAPDH initiates apoptotic cell death by nuclear translocation following Siah1 binding. *Nat Cell Biol* 7(7):665–674.
42. Kornberg MD, et al. (2010) GAPDH mediates nitrosylation of nuclear proteins. *Nat Cell Biol* 12(11):1094–1100.
43. Nott A, Watson PM, Robinson JD, Crepaldi L, Riccio A (2008) S-Nitrosylation of histone deacetylase 2 induces chromatin remodelling in neurons. *Nature* 455(7211):411–415.
44. Marino SM, Gladyshev VN (2010) Structural analysis of cysteine S-nitrosylation: A modified acid-based motif and the emerging role of trans-nitrosylation. *J Mol Biol* 395(4):844–859.
45. O'Shea JP, et al. (2013) pLogo: A probabilistic approach to visualizing sequence motifs. *Nat Methods* 10(12):1211–1212.
46. Stamler JS, Toone EJ, Lipton SA, Sucher NJ (1997) (S)NO signals: Translocation, regulation, and a consensus motif. *Neuron* 18(5):691–696.
47. Raju K, et al. (2015) Regulation of brain glutamate metabolism by nitric oxide and S-nitrosylation. *Sci Signal* 8(384):ra68.
48. Block E, Ofori-Okai G, Zubieta J (1989) 2-phosphino- and 2-phosphinylbenzenethiols: New ligand types. *J Am Chem Soc* 111(6):2327–2329.
49. Figuly GD, Loop CK, Martin JC (1989) Directed ortho-lithiation of lithium thiophenolate. New methodology for the preparation of ortho-substituted thiophenols and related compounds. *J Am Chem Soc* 111(2):654–658.
50. Wiśniewski JR, Zougman A, Nagaraj N, Mann M (2009) Universal sample preparation method for proteome analysis. *Nat Methods* 6(5):359–362.
51. Slade PG, et al. (2010) Proteins modified by the lipid peroxidation aldehyde 9,12-dioxo-10(E)-dodecenoic acid in MCF7 breast cancer cells. *Chem Res Toxicol* 23(3):557–567.
52. Ravindra KC, et al. (2015) Untargeted proteomics and systems-based mechanistic investigation of artesunate in human bronchial epithelial cells. *Chem Res Toxicol* 28(10):1903–1913.
53. Huang DW, et al. (2007) The DAVID Gene Functional Classification Tool: A novel biological module-centric algorithm to functionally analyze large gene lists. *Genome Biol* 8(9):R183.